AD-A076 541 VILLANOVA UNIV PA DEPT OF MECHANICAL ENGINEERING F/G 14/2
AERSTRUCTURE NONDESTRUCTIVE EVALUATION BY THERMAL FIELD TECHNI--ETC(U)
NOV 79 P V MCLAUGHLIN, E V MCASSEY N68335-78-M-5337
UNCLASSIFIED NAEC-92-131 NL

1 OF 1
AD
A076541

END
DATE
FILMED
12-79
DDC

LEVEL II (12)

NAVAL AIR ENGINEERING CENTER

REPORT NAEC-92-131

LAKEHURST, N.J. 08733

AD A076541

AEROSTRUCTURE NONDESTRUCTIVE EVALUATION BY THERMAL FIELD TECHNIQUES

Handling & Servicing/Armament Division
Ground Support Equipment Department
Naval Air Engineering Center
Lakehurst, New Jersey 08733

1 November 1979

Final Report for Period 17 March 1978 - 17 January 1979
AIRTASK A3400000/051B/8F41461406

APPROVED FOR PUBLIC RELEASE:
DISTRIBUTION UNLIMITED

Prepared for

Commander, Naval Air Systems Command
AIR-340E
Washington, DC 20361

NAEC-92-131

AEROSTRUCTURE NONDESTRUCTIVE EVALUATION BY THERMAL FIELD TECHNIQUES

Prepared by: P.V. McLaughlin

P. V. McLaughlin, Jr.
Dept. of Mechanical Engineering
Villanova University

E.V. McAssey Jr.

E. V. McAssey, Jr.
Dept. of Mechanical Engineering
Villanova University

R.C. Deitrich

R. C. Deitrich
Advanced Technology Section, Handling
and Servicing/Armament Division

Approved by: C.E. Campbell

C. E. Campbell, CAPT USN
Ground Support Equipment Officer

11/1/79 da

UNCLASSIFIED

SECURITY CLASSIFICATION OF THIS PAGE (When Data Entered)

19 REPORT DOCUMENTATION PAGE

READ INSTRUCTIONS BEFORE COMPLETING FORM

1. REPORT NUMBER: 18 NAEC-92-131

2. GOVT ACCESSION NO.

3. RECIPIENT'S CATALOG NUMBER

4. TITLE (and Subtitle): 6 Aerostructure Nondestructive Evaluation by Thermal Field Techniques.

5. TYPE OF REPORT & PERIOD COVERED: 9 Final rept. 17 Mar 78 - 17 Jan 79,

6. PERFORMING ORG. REPORT NUMBER

7. AUTHOR(s): 10 [redacted]. P. V./McLaughlin, Jr., [redacted]. E. V./McAssey, Jr. [redacted]. R. C./Deitrich*

8. CONTRACT OR GRANT NUMBER(s): 15 N68335-78-M-5337 new

9. PER[redacted]G ORGANIZATION NAME AND ADDRESS: Villanova University, Dept. of Mechanical Engineering, Villanova, Pa. 19085

10. PROGRAM ELEMENT, PROJECT, TASK AREA & WORK UNIT NUMBERS: A3400000/051B/8F41461406

11. CONTROLLING OFFICE NAME AND ADDRESS: Naval Air Systems Command, AIR-340E, Washington, D.C. 20361 — 12 38

12. REPORT DATE: 11 1 Nov[redacted]79

13. NUMBER OF PAGES: 40

14. MONITORING AGENCY NAME & ADDRESS (if different from Controlling Office): *Naval Air Engineering Center, Ground Support Equipment Dept. (Code 92724), Lakehurst, N.J. 08733

15. SECURITY CLASS. (of this report): UNCLASSIFIED

15a. DECLASSIFICATION/DOWNGRADING SCHEDULE

16. DISTRIBUTION STATEMENT (of this Report)

Approved for Public Release; Distribution Unlimited

16 F41461 17 WF41461406

17. DISTRIBUTION STATEMENT (of the abstract entered in Block 20, if different from Report)

18. SUPPLEMENTARY NOTES

19. KEY WORDS (Continue on reverse side if necessary and identify by block number)

Thermography; Infrared flaw detection; Nondestructive evaluation; Composite materials; Glass epoxy; Graphite epoxy

20. ABSTRACT (Continue on reverse side if necessary and identify by block number)

Certain types of flaws and damage in composite materials are not readily observable by visual examination. Examples of these are delaminations, blind-side impact damage, and sub-surface laminar cracks. Programs are currently underway to develop methods of detecting such flaws by many techniques, among which are X-ray, neutron radiography, ultrasonic transmission and reflectance, eddy current, and thermography. This report describes results of an experimental and analytical research investigation to evaluate infrared thermography

DD FORM 1 JAN 73 1473 EDITION OF 1 NOV 65 IS OBSOLETE
S/N 0102-LF-014-6601

UNCLASSIFIED

SECURITY CLASSIFICATION OF THIS PAGE (When Data Entered)

409 253

as an NDE tool to locate defects and structural damage which are not easily located by visual examination. Also discussed are possible applications to aluminum structures.

PREFACE

The Nondestructive Evaluation (NDE) of advanced aerostructural materials has been approached using many techniques; among these are radiography (both X-ray and N-ray), ultrasonics, eddy current, hallographics, etc. Recently, probably the most widely used is ultrasonics, especially for composite materials. Ultrasonics has many advantages; however, one disadvantage of the technique is the necessity for tedious scanning procedures in order to inspect large surface areas.

It is this disadvantage which has prompted this research into thermographic infrared detection of flaws which could provide a more rapid method of inspecting large aerostructural surfaces. Use of large surface areas of graphite epoxy is a certainty on advanced Naval aircraft. The F-18 Hornet, for example, is estimated to have about 40% of its external surface areas made of advanced composite materials.

Rapid scanning of such areas with thermographic techniques will most certainly lead to some loss of quantitative information; however, if potential flaw sites can be identified in a rapid manner, then another technique such as ultrasonics, could be used at the potential flaw locations to confirm flaw presence and quantify flaw extent. This procedure should significantly reduce inspection time when compared with ultrasonic scanning of the total surface. It is with this goal in mind that this research has been initiated.

Thanks are given to Mr. C. Chance of Grumman Aerospace Corp. and Dr. W. E. Dance of Vought Corp., Advanced Technology Center, for providing composite samples and to Dr. W. R. Scott of the Naval Air Development Center for his advice during this effort.

THIS PAGE LEFT BLANK
INTENTIONALLY.

TABLE OF CONTENTS

LIST OF ILLUSTRATIONS

LIST OF TABLES

I. INTRODUCTION

A. Certain types of flaws and damage in aerospace composite and aluminum structures are not readily observable by visual examination. Examples of these are delaminations, blind-side impact damage, and subsurface interlaminar cracks. Programs are currently under way to develop methods of detecting such flaws by many nondestructive evaluation (NDE) techniques, among which are X-ray, neutron radiography (N-ray), ultrasonic transmission and reflectance, eddy current, and thermography. This report describes results of an experimental and analytical research investigation to evaluate infrared thermography as an NDE tool for composite and aluminum structures to locate defects and structural damage which are not easily located by visual examination.

B. The nondestructive examination of materials and structures by infrared thermography has been investigated by several researchers (references (a) through (l), for example). Most of the recent work on composites (references (g) through (j), for example), has been directed toward detecting damage propagation in the vicinity of a flaw or crack in a composite structure under cyclic loading. The current investigation is aimed at utilization of perturbed thermal patterns in structures to locate such flaws. Two methods can be used to generate thermal fields to detect flaws, cracks, or damaged regions:

1. EXTERNALLY APPLIED THERMAL FIELD (EATF). An external heat source can be applied to structural surfaces in order to generate thermal gradients in the structure. If there are no flaws and the gradient is uniform, isotherms would be straight lines. Temperatures "downstream" of the applied heat source would also be uniform. In the presence of a flaw or damaged region, the discontinuous thermal conductivity would cause a perturbation in the heat flux and temperature field, resulting in curved isotherms and nonuniform temperatures "downstream" of the perturbation as shown in Figure 1.

2. STRESS-GENERATED THERMAL FIELD (SGTF). Even though most materials including metals and composites can be idealized as linear-elastic over a significant portion of their load range, there is always a hysteresis loop, however small, upon loading and unloading. The energy so generated in a cycle of loading and unloading is dissipated as heat, and the heat generated is highest where stresses and deformation are highest. Since cracks, flaws, and damaged regions will act as stress concentrators under applied stress, the heat generated in cycles of loading and unloading will be maximum where the stresses are highest...near the flaws. In polymeric composites, the matrix is of low conductivity and stress-strain characteristics cause a large hysteresis loop; hence the stress field near the flaws or cracks causes "hot spots" to develop in the region immediately adjacent to the flaw (Figure 2).

C. Reifsnider and Stinchcomb (reference (i)) have observed heat generation near damaged regions of an impacted graphite/epoxy laminate which was loaded cyclically at 45 Hz by a servo-hydraulic testing machine, but it is unclear whether the heat generation was due to continuing damage propagation or was only viscoelastic material behavior. They also describe a SGTF method of

inducing thermal hot spots in flawed specimens by inertial cyclic loading through a shaker or transducer (reference (i)). Recently, Henneke and Jones (reference (k)) have been able to show that hot spots are produced at delaminated areas of composite laminates which have been axially cycled with an ultrasonic vibrator. Also, Charles (reference (l)) has described the use of liquid crystals to detect flaws by both SGTF and EATF techniques.

D. The present program has investigated the practicality of detecting damage sites or flaws in composite structures using an infrared camera with video-isotherm readout. Both EATF and SGTF techniques were evaluated. Various specimens, both flawed and intact, were subjected to EATF and SGTF heat generation. Photographs of the resulting temperature fields were taken for several types and sizes of flaws in graphite/epoxy, glass/epoxy, boron/epoxy, and aluminum specimens. Concurrently, analytical thermal field calculations were made and checked against the tests to explain results obtained and point out factors which affect successful thermographic detection of flaws in composites. These preliminary results have allowed an assessment to be made of the feasibility of development of thermographic techniques and equipment for use in the Naval aviation maintenance environment. Tentative conclusions concerning hardware required for thermographic NDE have also been drawn.

II. EQUIPMENT AND PROCEDURES

A. Defects were implanted in plates of laminated graphite/epoxy, boron/epoxy, glass/epoxy, and 6061-T6 aluminum. Since 6061-T6 and graphite have nearly the same conductivity (150 W/m °C), a composite of graphite and aluminum will exhibit very little anisotropy in thermal conductivity, and will have about the same conductivity as the aluminum alone. Thermal NDE results for aluminum specimens are therefore expected to represent those of graphite/aluminum metal matrix composites.

B. Temperature gradients were induced in all specimens by applying heat externally (EATF) or by stress-cycling (SGTF). The resulting transient surface temperatures were monitored by an AGA Thermovision System 680/102B infrared camera with both black and white and color isotherm video readout.

1. A uniform temperature gradient would be indicated on the black and white screen as a continuous change of shade from white (hottest) to black (coolest).

2. The color television screen breaks a given range of temperatures down into ten sub-ranges, and shows each 1/10 of the total temperature range as a different color. For example, a 10°C gradient from 20°C to 30°C would show up on the color screen at 10°C sensitivity as:

COLOR	TEMPERATURE (°C)	COLOR	TEMPERATURE (°C)
White	above 29	Light Blue	23-24
Yellow	28-29	Green	22-23
Orange	27-28	Blue Green	21-22
Red	26-27	Dark Blue	20-21
Lavender	25-26	Black	Below 20
Purple	24-25		

As a result, borders between colors represent isotherms (for example: the border between orange and red indicates surface temperatures of 27°C). Perturbations in otherwise smooth isotherms as shown in Figure 1 indicate the presence of flaws interrupting otherwise uniform heat flow for EATF methods, and hot spots or concentric closed isotherms indicate stress concentrations for the SGTF heat generation of Figure 2. Since exact temperatures are not necessary for identifying defects by perturbed isotherms, most photographic records of the color video screen were taken in black and white. The resulting isotherm bands are sufficiently distinct to locate defect-induced perturbations.

C. Types of defects investigated were: delaminations, partial through-cracks, through-holes, and partial through-holes. (The latter were used to simulate blind-side impact damage where the impacted surface shows no sign of damage, but the back side can be shattered or severely damaged by reflected stress waves.) Some preliminary testing was also done on riveted aluminum joints. Thermal gradients were induced in samples by conduction and

radiation/convection EATF methods, and by tension-tension cycling with an Instron test machine to induce SGTF isotherms. In addition, tests were conducted to assess the importance of emissivity, reflectivity, and conductivity for various painted and unpainted surfaces. Finally, an assessment was made of the need for several equipment features such as temperature level adjustment, temperature sensitivity range, type of heat source and application technique, and type of video thermal readout. Table 1 lists the tests performed and materials used.

TABLE 1 - THERMOGRAPHIC TEST PROGRAM OUTLINE

TEST TYPE		MATERIALS, PARAMETERS TESTED		
		EATF METHOD		SGTF METHOD
	FLAW TYPE	CONDUCTION	RADIAT./CONVECT.	CYCLIC TENSION
FLAW DETECTION	THRU-HOLE	Gr/Ep,B/Ep, Gl,Ep,Al	-	Gr/Ep,Gl/Ep,Al
	PART THRU-HOLE	Gr/Ep	Gr/Ep Gl/Ep	Gr/Ep,Gl/Ep
	DELAMINATION	Gr/Ep,Gl/Ep	Gr/Ep,Gl/Ep	-
	PART THRU-CRACK	Gr/Ep	Gr/Ep	Gr/Ep
	RIVETED JOINTS	Al	-	-
SURFACE CHARACT'S	SURF. REFLECTION	Painted/unpainted Al, Gr/Ep, B/Ep, Gl/Ep		
	SURF. EMISSIVITY	Black/white painted Al, Unpainted Gr/Ep,B/Ep,Gl/Ep		
	MTL. CONDUCTIVITY	Directional Gr/Ep,Gl/Ep,B/Ep; Aluminum		
EQUIPMENT FEATURE & PARAMETERS TEST		Temp. level adjustment, temp. sensitivity range, heat source/application technique, video readout		

D. For the EATF tests, two heat generation techniques were used as shown in Figure 3. In the conduction technique, a 6-x-6-inch (15.2 cm x 15.2 cm) specimen was clamped between insulated supports with the test section below the supports. The top section (above the supports) was heated continuously with an electrical heat gun. Heat was conducted down the specimen into the test section causing transient thermal gradients in the plane of the specimen surface. The radiation/convection heat application technique utilized the same low air volume heat gun with 350-600 watt electrical resistance heater elements. Heat was radiated and convected directly onto the test section surface, causing transient thermal gradients perpendicular to the surface as well as parallel to the surface.

E. SGTF heat was generated in flawed specimens by cycling in a tension-tension mode (R=0.1, 0.5 to 5 Hz) at maximum average stress levels representing 0.05, 0.10, 0.20, 0.30, and 0.50 of the flawed specimen's ultimate static failure load. Figure 4 shows a schematic diagram of the SGTF test setup. Results of previous investigations (references (h) through (k) for example) have shown that heat is generated near flaws in composite specimens at 0.2 to 0.8 of the static ultimate load and at cyclic frequencies of 15 to 50 Hz. The present program investigated significantly lower maximum loads and cyclic frequencies.

III. EATF FLAW DETECTION TEST RESULTS

A. THROUGH-HOLES

1. A hole which extends completely through the thickness of a plate can be easily seen and, of course, needs no NDE by any means other than the naked eye. It is, however, a convenient simulation of other defects such as impact shattering, and provides an easily manufactured flaw for a testing program. Therefore, to shed light on the effects of material properties, surface characteristics, heat application techniques, etc., holes ranging in size from 1/64 to 1 inch (0.04 to 2.54 cm) in diameter were drilled in .06-inch to 1/8-inch (0.15 cm to 0.32 cm) thick plates of [0] Gr/Ep (graphite/epoxy), [0] B/Ep (boron/epoxy), [0/90] Gl/Ep (glass/epoxy), and 6061-T6 aluminum. The plates were mounted in the frame shown schematically in Figure 3 and heated.

2. Typical results for the conduction experiments are shown in Figure 5. For the unidirectional graphite/epoxy specimens, orientation of fibers to the heat flow direction had a large effect upon the degree of isotherm perturbation. In all three cases (fibers parallel, perpendicular, and at 45 degrees to heat flux) there was a definite "hourglass" perturbation around the flaw as regions upstream of the flaw heated more quickly and regions downstream of the flaw heated less quickly than the unflawed portions of the plate on either side. However, the perturbation was greatest for the specimen with fibers parallel to the heat flux direction and least for fibers at 90 degrees. This was expected, since graphite/epoxy exhibits a high degree of anisotropic thermal conductivity, K (about 80 W/m^{o}C in the fiber direction, and 0.5 W/m^{o}C transverse to the fibers). Note the skewed isotherm pattern in the 45-degree orientation. Unidirectional glass/epoxy is thermally less anisotropic (K_{axial} = 0.7, K_{trans} = 0.3 W/m^{o}C), and the cross-plied laminate tested had a thermal conductivity about equal to the transverse conductivity of the [0] GR/Ep. As seen in Figure 5, the [0/90] Gl/Ep exhibits about the same isotherm perturbations as does the 90^{o} Gr/Ep. Boron/epoxy has an axial conductivity between those of Gr/Ep and Gl/Ep, and the perturbations in the [0] and [45] B/Ep isotherms of Figure 5 are greater than those for glass but less than those for Gr/Ep. Isotherm perturbations for heat conduction transverse to fibers was about the same for B/Ep as for Gr/Ep and Gl/Ep.

3. Aluminum was used to simulate graphite/aluminum metal matrix composites. Perturbed isotherms for the aluminum samples looked much like the graphite/ and boron/epoxy results with distinct "hourglass" isotherm perturbations. Results are shown in Figures 6 and 7 for IR camera sensitivities of 5^{o} C and 2^{o} C, respectively, with hole diameters from 1/64 inch (0.04 cm) to 1/2 inch (1.27 cm). Note that hole diameters of 1/16 inch (0.16 cm) and less did not cause visible perturbations in the isotherm pattern, while hole diameters of 1/8 inch (0.32 cm) and larger resulted in visible isotherm perturbations. Also, while 2^{o} C IR camera sensitivity settings (Figure 7) resulted in more isotherms than the 5^{o} C sensitivity results (Figure 6), the isotherms in the 2^{o} C results were less distinct and showed "fuzzy" boundaries between colors.

B. DELAMINATIONS. Edge delaminations were placed in Gr/Ep and Gl/Ep plates. Both conduction and radiation/convection tests were performed.

1. The upper half of Figure 8 shows results of conduction tests on Gr/Ep. The left-hand picture was taken as heat propagated parallel to fibers from the right side. Note the "spike" at the bottom edge of the plate at the exact location of the edge delamination, and the coolness of the free edge where considerable heat is being lost by surface convection. The upper right shows results of heat being conducted transversely to the fiber direction. Note the hot spot at the edge in the delaminated regions.

2. An edge split was placed in [0] Gr/Ep (lower left, Figure 8) by peeling up a 1/2-inch-wide by 1/32-inch-deep by 1-inch-long strip. Hot air was radiated/blown onto the surface to the right of the split with a heat gun, resulting in the isotherm pattern shown. Note that the flaw characteristics are neatly outlined by the isotherm pattern.

3. The lower right photo in Figure 8 illustrates the effect of heating a [0/90] Gl/Ep plate containing a triangular edge delamination at mid-plane. The resulting isotherm pattern not only clearly locates the flaw, but outlines its boundaries accurately.

C. PARTIAL THROUGH-HOLES. When composite surfaces are impacted with low-velocity blunt objects, many times the back surface shatters but there is no visible damage on the front surface. To roughly approximate this type of damage, 1/4-inch-diameter (0.64 cm) holes were drilled about 50 percent through 0.1-inch-thick (0.25 cm) plates of Gr/Ep and Gl/Ep. Both conduction and radiation/convection tests were performed with the unflawed surface facing the infrared camera.

1. In the conduction tests (top of Figure 9), an hourglass isotherm perturbation pattern was visible in the Gr/Ep at the flaw location. The patterns were much like those which developed around the through-holes, and clearly indicated the presence of the flaw.

2. For the radiation/convection tests, a heat gun was held at 3 inches (7.62 cm) from the specimen surface and moved from left to right at a velocity of 2 inches per second (5.08 cm/sec). At the location of the partial through-hole, a distinct hot spot appeared as shown in Figure 9, lower left, for a Gr/Ep specimen. Similar results were obtained for Gl/Ep specimens. To evaluate the effects of cooling from a higher temperature, a cool, damp cloth was wiped across the specimen's surface. The resulting thermal image is shown in Figure 9, lower right. Note, in addition to the black spot at the defect location, there is a set of peaks or corners in the isotherm pattern running upwards from the left of the black spot. Upon close visual inspection, it was determined that a part-through surface crack had been imparted to the specimen, probably during the drilling operation. The interruption in thermal conductivity due to the crack had caused a discontinuity in isotherms as heat from the hotter upper left-hand portion of the specimen (white on the photograph) propagated downward.

D. PARTIAL THROUGH-CRACKS. Several conduction tests were performed on Gr/Ep samples with partial through-cracks parallel to the fiber direction. It was found that these cracks could best be detected by heat flux direction perpendicular to the cracks, or at an angle greater than 45 degrees to the crack. Thermal patterns looked much like those shown in Figure 9 lower right or in Figure 8 lower left, and indicated both location and extent of the cracks.

E. RIVETED ALUMINUM JOINTS. A six-rivet, aluminum butt joint was fabricated from 0.060-inch (1.5 mm) sheeting and pop-rivets as shown in Figure 10. The joint was secured in the conduction test rig (Figure 3) and heated from the top. Test results are shown in Figure 10, where the right-hand photograph was taken 60 seconds after the left-hand photograph. Interestingly, the top main plate heated rapidly, but the cover plate on the front heated very slowly, and never reached the other's high temperature. Also, the two top rivets heated more rapidly than the cover plate. Close visual inspection revealed that the riveted joint was not tight; that is, there was an air gap between the top main plate and the cover or lap plates, and the third rivet was loose. This resulted in little heat being transferred to the cover plate directly from the top main plate, and prevented the third rivet from conducting any significant heat to the front surface. These results, although preliminary, indicate that thermography might be used for inspection of integrity of riveted joints in aircraft structures.

IV. SGTF FLAW DETECTION TEST RESULTS

A. Even at the relatively low frequencies of testing (0.5 to 5 Hz), cyclic tensile loading was able to cause detectable heat patterns in [0/90] glass/epoxy laminates. Figure 11, top left, shows hot-spot isotherms generated in the vicinity of a 1/4-inch diameter (0.64 cm) hole drilled 75 percent through from the back surface of the specimen. Visible heat was generated after only 30 cycles at 1 Hz and 0.1 of the flawed specimen static failure load. This was typical of results of Gl/Ep samples containing partial through-holes and through-holes.

B. Attempts to generate heat in graphite epoxy at the low cyclic frequencies was at first unsuccessful, as had been similar tests by other researchers. The lower left photograph in Figure 11 shows a unidirectional Gr/Ep specimen with a 1/4-inch-diameter (0.64 cm) through-hole after having been subjected to 1,000 cycles at each of 0.05, 0.1, 0.2, 0.3 static ultimate loads. Even though some slight temperature rise is observed near the grips due to the high shear strains in the glass/epoxy end tabs, no temperature change is visible near the hole. After about 400 cycles at 0.4 static ultimate, a sharp noise or "ping" emanated from the specimen. The picture in Figure 11 lower right was taken 50 cycles after the noise was heard, and sharp "spikes" of temperature were observed. The test was stopped, and the specimen inspected. Two through-cracks were found running from the sides of the hole into the grips, and were located in the middle of the heated area observed with the infrared camera. Since it was uncertain whether the heat had been due to liberated energy from the fracture or frictional dissipation due to the rubbing of the opposing crack surfaces, the specimen was allowed to cool. The sample was retested at 0.1 static ultimate and 1 Hz, and visible heat spikes developed after about 15 cycles. A second test sample was tested, this time with a 1/4-inch (0.64 cm) slit or crack cut 50 percent through the back surface, perpendicular to the load direction. The test sequence was identical to the one used for the through-hole, and the specimen was monitored closely to observe crack initiation and propagation. Again, no visible heat was generated until 150 cycles at 0.3 static ultimate, when the "ping" was heard. No heat was immediately visible. Fifteen cycles after the "ping", the spikes shown in Figure 11 were observed. The test was stopped, the specimen was allowed to cool, and then retested at 0.3 static ultimate and 1 Hz. The heat spikes reappeared after 15 cycles. It is concluded that no significant heat was liberated from the fracture, and that the friction was the source of the observed heat spikes. It is noted that Whitcomb (reference (j)) has observed similar heating effects in cycled specimens of damaged boron/epoxy.

C. Attempts to generate visible heat in flawed aluminum specimens at low frequencies were unsuccessful, even beyond the elastic limit of the material. This is most likely due to the small amount of generated heat being quickly conducted away from highly stressed regions.

V. EFFECTS OF SURFACE CHARACTERISTICS

A. REFLECTIVITY.

1. During initial tests on unpainted aluminum specimens, it was noted that occasional spurious hot spots could be seen on the IR camera video screen. Investigation uncovered that radiated body heat could reflect from the highly reflective aluminum surface. Figure 12 (top) shows a technician's index finger held 1/16 inch (0.16 cm) from the edge of an aluminum specimen. Note the reflected hot spot at the left-hand edge of the specimen. Shown for comparative purposes are the color band isotherm video picture (left) and the continuous shade black and white (gray scale) video picture (right). The lower half of Figure 12 shows the heat reflected from an ignition key which had been warmed on one side by body heat. Similar results have been obtained for light bulbs, radiant heaters, etc., as far as 20 feet (6.1 m) away from the specimen. Obviously, surface reflectance characteristics and ambient conditions must be taken into account if reliable NDE is to be performed with IR thermography.

2. The right-hand photograph in Figure 13 shows the thermographic picture obtained on an aluminum specimen similar to that shown in Figure 12, except that the Figure 13 specimen had been spray painted with black and white flat enamel. A technician's arm was held near the specimen in a position that had caused a significant hot spot to be reflected from an unpainted aluminum specimen. Note that there is virtually no reflection from either the black or white sides.

3. Similar tests were conducted on Gr/Ep, B/Ep, and Gl/Ep. No visible reflected heat was observed for these composites, even when surfaces were unpainted.

B. EMISSIVITY. Emissivity quantifies the ability of a surface to radiate heat: high emissivity surfaces emit more heat; low emissivity surfaces emit less heat. Since composite structures will most likely be painted or otherwise finished, it is desirable to know what effect, if any, different paint colors or types may have on results of thermal scanning. The same half-black, half-white painted specimen used for reflectivity tests was secured in the conduction test stand (Figure 3) and heated at the top. Results of the transient isotherm pattern are shown in Figure 13, left. Note that there is no difference in isotherm pattern for the two paints.

C. CONDUCTIVITY.

1. It has already been noted that for EATF conduction tests, anisotropy of conductivity has an effect upon the degree of isotherm perturbation in the vicinity of a flaw; heat flow parallel to high conductivity fibers results in the greatest perturbations (see Figure 5). Also, it is more difficult to obtain a significantly perturbed pattern in the low conductivity "isotropic" materials ([0/90] Gl/Ep) than in the high conductivity isotropic materials (aluminum). In the low conductivity materials, isotherms were much more closely spaced indicating a higher thermal gradient in the direction of heat flow, and the extent of the perturbation was not as extensive. In all tests,

it was observed that specimen edges were always cooler, indicating significant convective heat loss at free surfaces.

2. To examine this effect more closely a heat transfer analysis of a wide, flat plate was conducted. One edge was maintained at a constant temperature, and free-surface convection was allowed from both top and bottom surfaces. The steady-state temperature distribution was calculated as a function of plate length for thermal conductivities of K = 0.5 and 150 W/m ^{o}C, and results are shown in Figure 14. Note that effectively all of the heat input is lost from both plates in a finite distance, but the higher conductivity material has a smaller temperature gradient and heat is spread out over a considerably larger distance than for the lower conductivity materials. It appears that the higher gradients for low conductivity materials not only cause smaller perturbations in isotherms, but also cut down the effective distance over which a particular conductivity test can be conducted.

VI. EQUIPMENT CONSIDERATIONS

The particular infrared camera equipment used in this investigation was fairly sophisticated and had considerably more options than necessary for effective use in NDE of composite structures. The current investigation has pointed out several areas where simplification can be made, and other features which should remain substantially the same:

A. VIDEO DISPLAY. Considerably better definition of thermal field perturbations was obtained from the color isotherm screen than from the black and white continuous shade screen. Color was not essential, since flaws appeared as distinctly on the black and white photographs as they did on the color screen. Figure 15 presents a direct comparison of black and white versus color photographs of an SGTF test at 1^{o} C sensitivity. Note that the frictional heat dissipated along cracked surfaces extending from the hole are especially visible in both photographs. It is suggested that alternating black/grey/white strips might be used in place of color to reduce equipment cost.

B. TEMPERATURE SENSITIVITY RANGE. For the types of heat generation techniques used in this study, temperature sensitivity ranges with full-scale readings of 1, 2, and 5^{o} C gave the best identifiable isotherm readouts. A comparison of perturbed isotherms around a 1/2-inch diameter hole in black-painted aluminum for sensitivity ranges of 1 to 50^{o} C is shown in Figure 16. Note that curved isotherms can clearly be seen in the 1, 2, and 5^{o} C ranges; little curvature in the 10^{o} C range, and none in the 20 or 50^{o} C ranges. Although some sensitivity adjustment will be desirable, perhaps the ranges of 10^{o} C and above can be excluded for NDE purposes.

C. TEMPERATURE LEVEL ADJUSTMENT. Ambient temperature will change with season and geographic location, and an increase in specimen temperatures normally occurs during individual NDE tests. It therefore appears that the temperature level adjustment, used to place the IR camera range within the range of temperature of a specimen during testing, will need to be retained.

D. HEAT APPLICATION TECHNIQUE. A heat gun can be used to generate heat both for conduction parallel to the surface and for radiation/convection normal to the surface. Figure 17 shows conduction tests for a 1/4-inch-diameter (0.62 cm) through-hole in a 1/8-inch-thick (0.32 cm) [0] boron/epoxy specimen. The left-hand photo was taken for the standard conduction test of Figure 3 (top), while the right-hand photo illustrates the results of heating the specimen from the bottom with a 350-watt heat gun. Even though isotherms away from the flaw generated by the heat gun are gently curving (right), the isotherm pattern is significantly perturbed in the vicinity of the flaw. Because of the heat gun's portability and ease of handling, it has advantages over a strip or blanket heater which must be secured to structural surfaces. Although further work needs to be performed on strip heaters, heat lamps, heat guns, etc., the portable hand-held heat sources seem to be preferable in the Naval Aviation Maintenance environment.

VII. CONCLUSIONS

A. The preliminary investigation described in this report has shown that infrared thermography is a strong candidate for development as an NDE tool for naval aviation maintenance applications. EATF techniques have been successful with Gr/Ep, Gl/Ep, B/Ep, and aluminum materials. Conduction tests have been able to locate delaminations, partial through-holes, surface cracks, and loose riveted joints; while radiation/convection tests using a heat gun have located partial through-holes and delaminations. SGTFs have been obtained in Gl/Ep at cyclic frequencies as low as 1 Hz and 0.05 of static ultimate load. No observable heat was generated in Gr/Ep or aluminum with stress concentrations such as holes or notches, but axially cracked Gr/Ep generated frictional heat between sliding crack surfaces, resulting in patterns visible with the IR camera. More work is necessary to define the limits of size, location, and type of defect that can be detected by thermography.

B. Surface reflectivity and conductivity can affect results; painted surfaces reduce spurious reflections. The color of paint had no visible effect upon isotherm patterns for the limited tests run. Further tests need to be performed for a wider range of paint types and colors, and to determine if soiled or abraded surfaces alter results.

C. It is clear that frequencies higher than 1 to 5 Hz are necessary to develop SGTF heat patterns in Gr/Ep and aluminum. Perhaps frequencies between those obtainable from servo-hydraulic test machines (50 Hz) and ultrasonic frequencies would be optimum. This is especially important since the load levels required to produce detectable heat at lower frequencies may cause damage propagation or reduction in structural lifetime under fatigue loading (references (h) and (j)).

D. Thermography has the potential to examine large surface areas rapidly, without the need for sophisticated data reduction and interpretation. Results of this investigation indicate that delaminations, blind surface impact damage, and surface cracks can be detected by infrared thermal field techniques.

E. Further work is warranted to determine ranges of flaw types, flaw sizes, flaw location, and structural materials that can be identified by both EATF and SGTF techniques. Also, both EATF and SGTF methods and heat application techniques need to be developed and refined to delineate the best system combinations for equipment development, and to determine effects of structural surface conditions (paint, dirt, oil, etc.) which occur in the naval aviation environment. Of special importance is the determination of whether SGTF methods using cyclic loads will degrade strength of structural systems during testing.

VIII. RECOMMENDATIONS

A. Pursue additional thermographic tests to:

1. Determine ranges of flaw types, flaw sizes, flaw location, and structural materials that can be identified by both EATF and SGTF techniques.

2. Determine the surface reflectivity and emissivity of a wider range of paint types and colors.

3. Determine if soiled or abraded surfaces alter results.

4. Determine the optimum frequency to develop SGTF patterns in Gr/Ep and aluminum.

5. Determine whether SGTF methods using cyclic loads will degrade strength of structural systems during testing.

IX. REFERENCES

(a) Apple, W. R., "Infrared Nondestructive Inspection Techniques", Presented at American Society for Quality Control Conference, Philadelphia, May 1968.

(b) Vogel, P. E. J., "Evaluation of Bonds in Armor Plate and Other Materials Using Infrared NDT Techniques", AMMRC TR 69-05, 1969.

(c) Vogel, P. E. J., "Nondestructive Testing of Tires, Parts I and II", Rubber Age, Nov and Dec 1974.

(d) Vicki, F. J., "Infrared Method for Detection of Inhomogenieties in Titanium", Pratt & Whitney Aircraft Report, Sep 1969.

(e) Pontello, A. P., "Development of NDE/I for Integral Wing Fuel Tank Structures using Infrared Thermography", Report No. NAPTC-PE-32, Jan 1974.

(f) Carlomagno, G. M., and Berardi, P. G., "Unsteady Thermotopography in Nondestructive Testing", Proceedings, Infrared Information Exchange, 1976.

(g) Indap, R. P., "Infrared Detection of Damage in Dynamically Loaded Fiberglass/Epoxy Panels", QTR No. 8-24000-2, Boeing-Vertol, 16 Dec 1974.

(h) Reifsnider, K. L., and Williams, R. S., "Determination of Fatigue-Related Heat Emission in Composite Materials", Experimental Mechanics, V. 14, No. 12, Dec 1974, p. 479.

(i) Reifsnider, K. L., and Stinchcomb, W. W., "New Methods of Mechanical Materials Testing Using Thermography", Proceedings, Infrared Information Exchange, 1976.

(j) Whitcomb, J. D., "Thermographic Measurement of Fatigue Damage", NASA Technical Memorandum 78693, May 1978.

(k) Henneke, E. G., II, and Jones, T. S., "Detection of Damage in Composite Materials by Vibrothermography", ASTM Committee D-30 Conference on NDE and Flaw Criticality for Composite Materials, Philadelphia, 10-11 Oct 1978.

(l) Charles, J. A., "Liquid Crystals for Flaw Detection in Composites", ASTM Committee D-30 Conference on NDE and Flaw Criticality for Composite Materials, Philadelphia, 10-11 Oct 1978.

THIS PAGE LEFT BLANK
INTENTIONALLY.

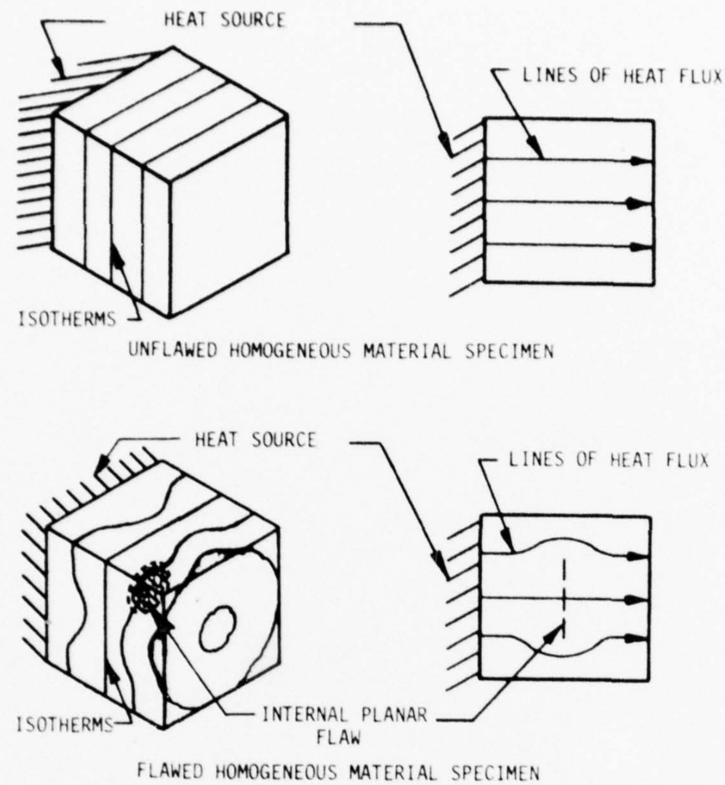

FIGURE 1 - COMPARISON OF TEMPERATURE FIELDS IN MATERIAL WITH AND WITHOUT INTERNAL FLAWS, EXTERNALLY APPLIED THERMAL FIELD

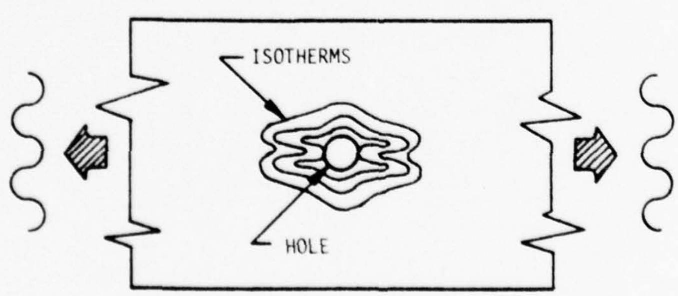

FIGURE 2 - SCHEMATIC OF OBSERVED TEMPERATURE FIELD IN A FLAWED ($0_2/\pm$ 45) BORON/EPOXY COMPOSITE MATERIAL TENSILE SPECIMEN UNDER CYCLIC LOADING-STRESS-GENERATED TEMPERATURE FIELD (SGTF)

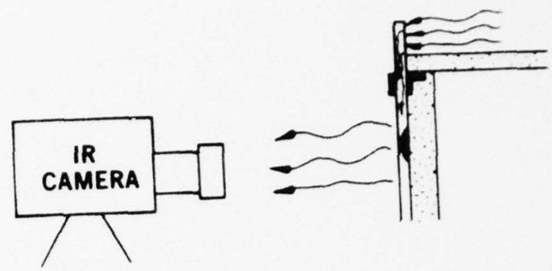

CONDUCTION

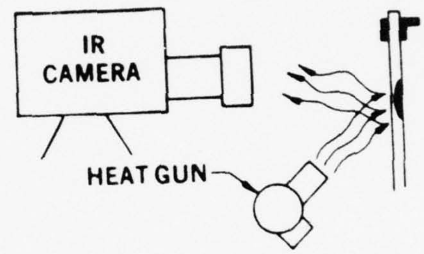

CONVECTION/RADIATION

FIGURE 3

SCHEMATIC DIAGRAM
OF EXTERNALLY APPLIED
THERMAL FIELD (EATF)
TEST SETUPS

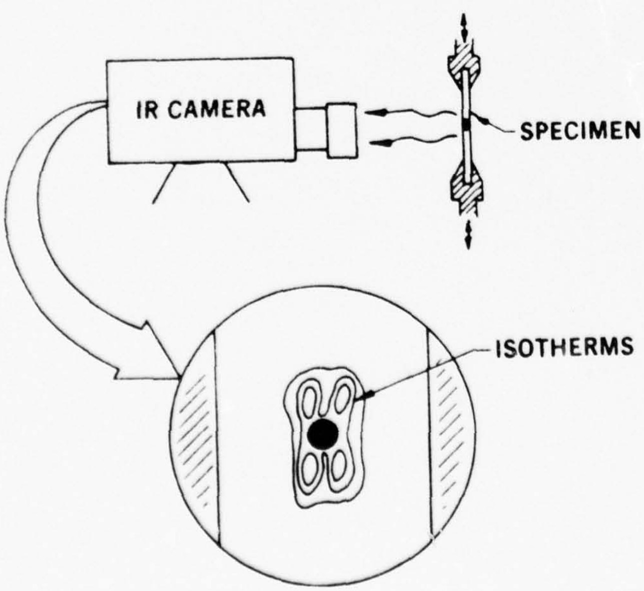

FIGURE 4

SCHEMATIC DIAGRAM
OF STRESS GENERATED
THERMAL FIELD (SGTF)
TEST SETUP

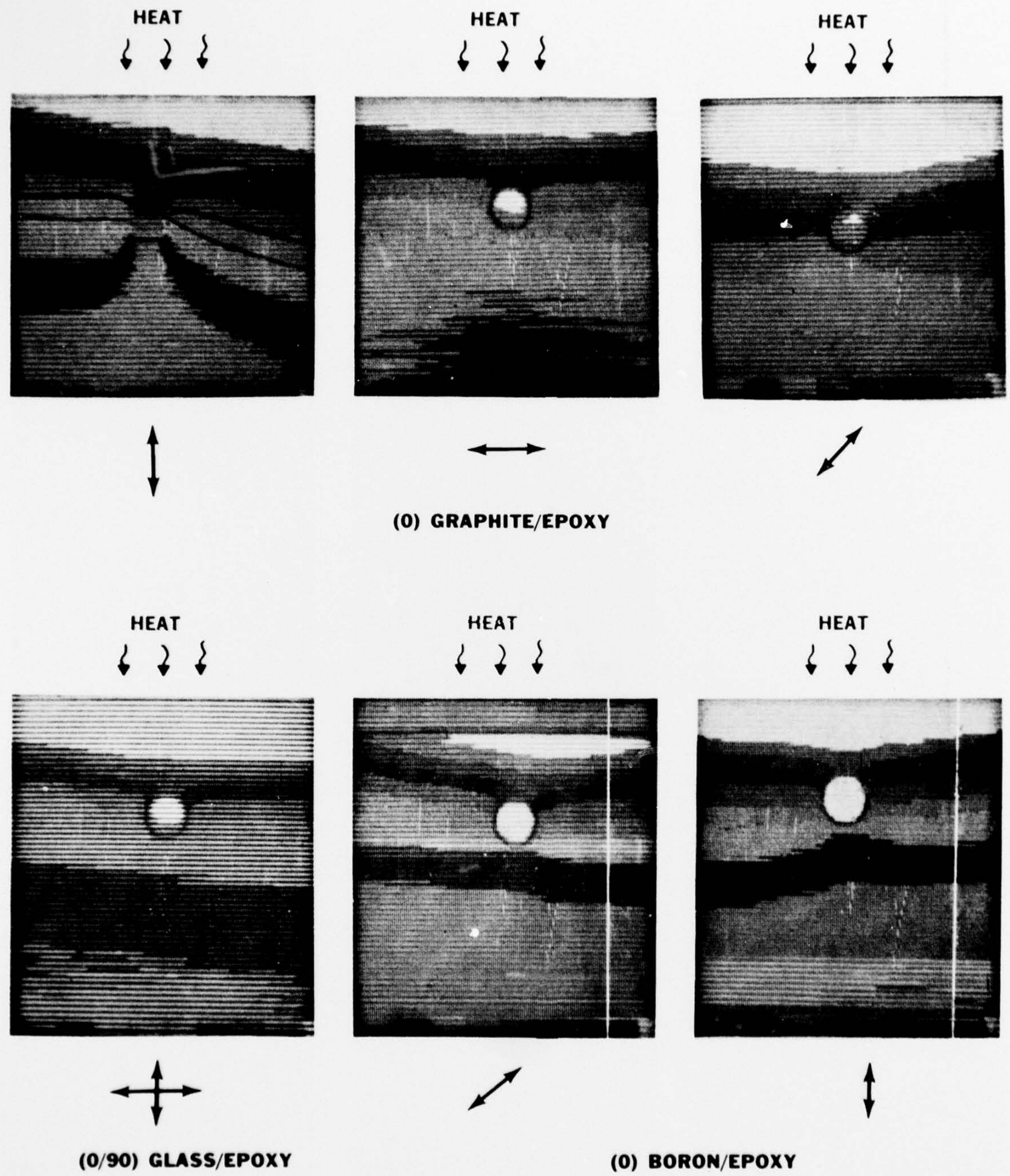

NOTE: Arrows under plates indicate fiber directions. Heat conducted from top of specimens.

FIGURE 5 - PERTURBED ISOTHERM PATTERNS AROUND 1/4-INCH-DIAMETER (0.63 CM) THROUGH-HOLE IN COMPOSITE PLATES, EATF

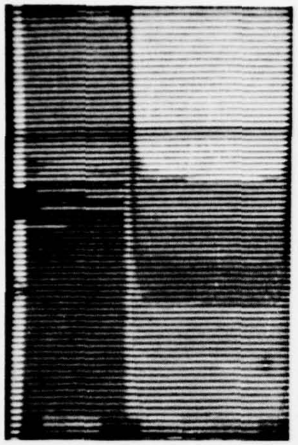

1/64-IN.-DIA HOLE
SENSITIVITY 5° C

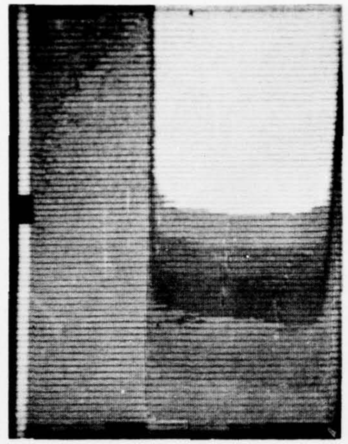

1/32-IN.-DIA HOLE
SENSITIVITY 5° C

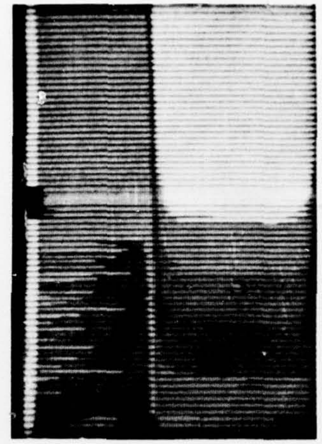

1/16-IN.-DIA HOLE
SENSITIVITY 5° C

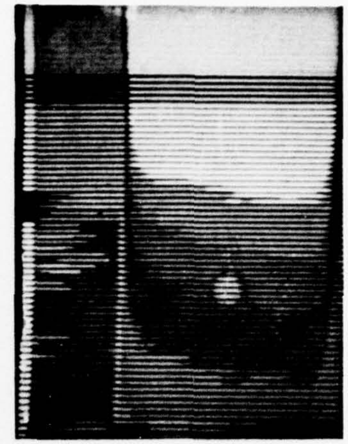

1/8-IN.-DIA HOLE
SENSITIVITY 5° C

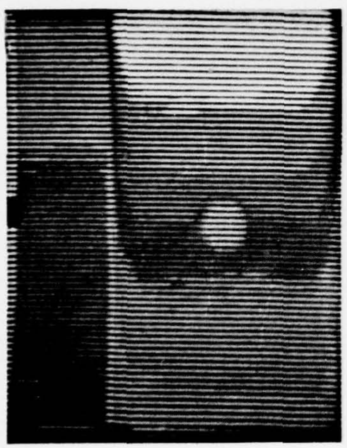

3/16-IN.-DIA HOLE
SENSITIVITY 5° C

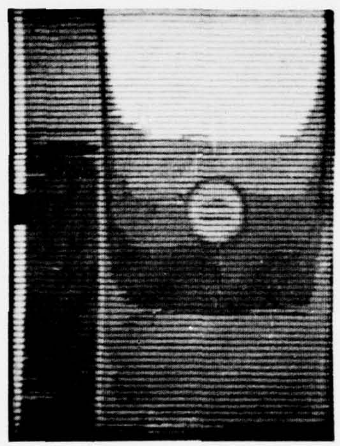

1/4-IN.-DIA HOLE
SENSITIVITY 5° C

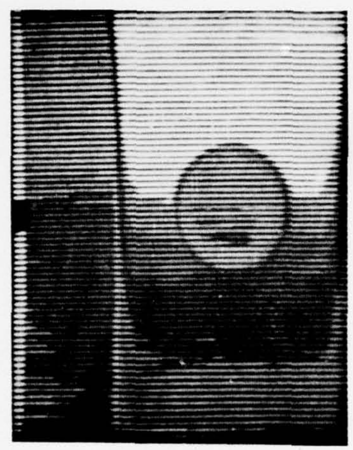

1/2-IN.-DIA HOLE
SENSITIVITY 5° C

FIGURE 6

EATF CONDUCTION RESULTS FOR BLACK ALUMINUM WITH 1/64- TO 1/2-INCH-DIAMETER THROUGH-HOLES, 5° C IR SENSITIVITY

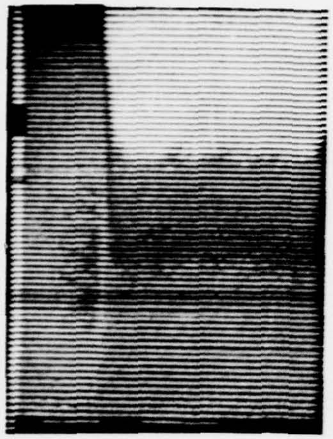

1/64-IN.-DIA HOLE
SENSITIVITY 2° C

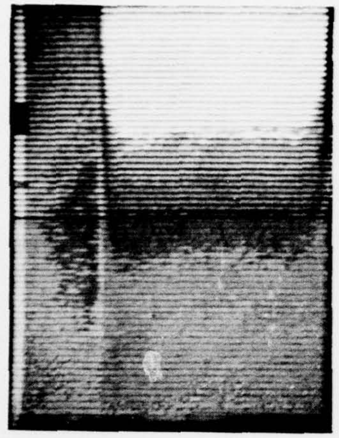

1/32-IN.-DIA HOLE
SENSITIVITY 2° C

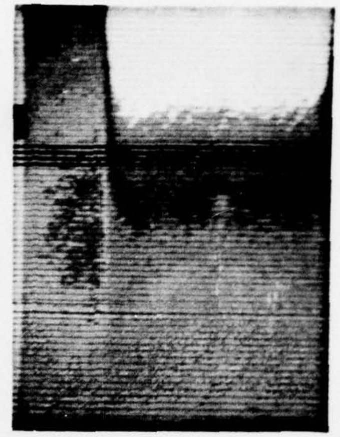

1/16-IN.-DIA HOLE
SENSITIVITY 2° C

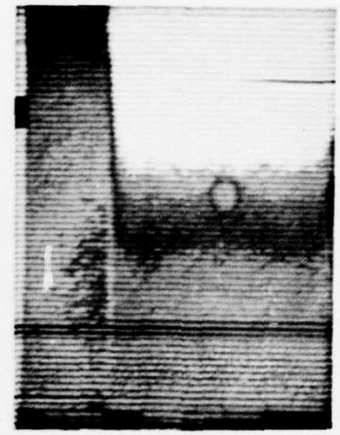

1/8-IN.-DIA HOLE
SENSITIVITY 2° C

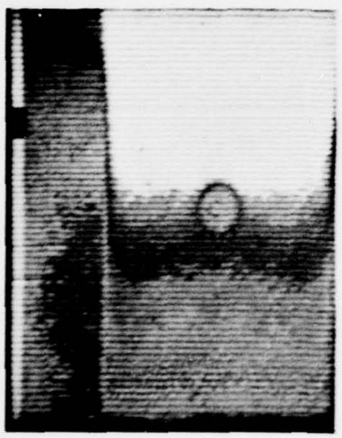

3/16-IN.-DIA HOLE
SENSITIVITY 2° C

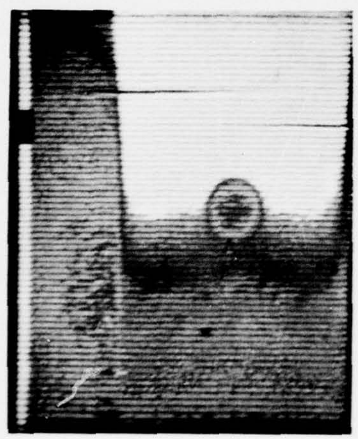

1/4-IN.-DIA HOLE
SENSITIVITY 2° C

1/2-IN.-DIA HOLE
SENSITIVITY 2° C

FIGURE 7

EATF CONDUCTION RESULTS FOR BLACK ALUMINUM WITH 1/64- TO 1/2-INCH-DIAMETER THROUGH-HOLES, 2° C IR SENSITIVITY

CONDUCTION

BOTTOM EDGE
HEAT CONDUCTED FROM RIGHT EDGE

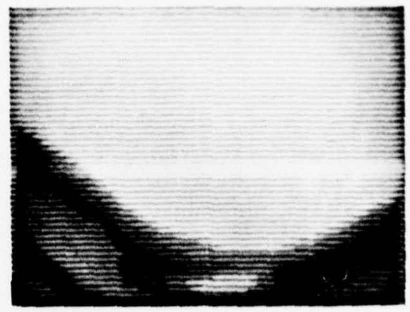

BOTTOM EDGE
HEAT CONDUCTED FROM TOP EDGE

(0) GRAPHITE EPOXY

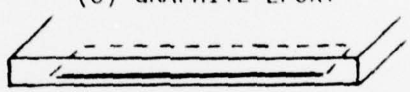

RADIATION/CONVECTION

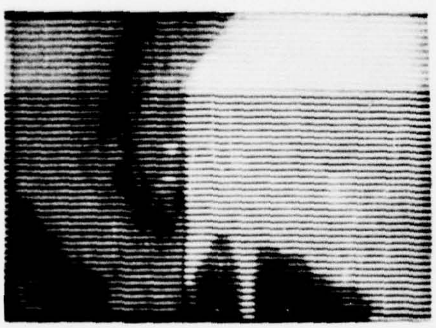

BOTTOM EDGE
SURFACE HEATED WITH HEAT GUN

(0) GRAPHITE EPOXY - EDGE SPLIT

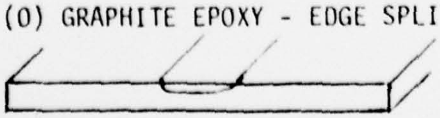

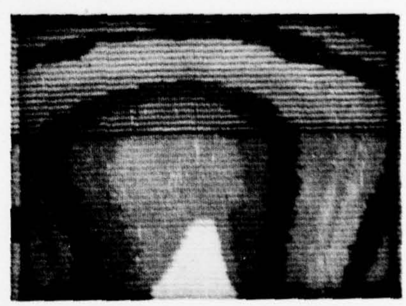

BOTTOM EDGE
SURFACE HEATED WITH HEAT GUN

(0/90) GLASS EPOXY - DELAMINATION

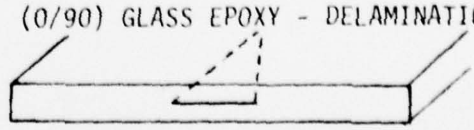

FIGURE 8 - PERTURBED ISOTHERM PATTERNS AND "HOT SPOTS" IN DELAMINATED COMPOSITE PLATES, EATF

CONDUCTION

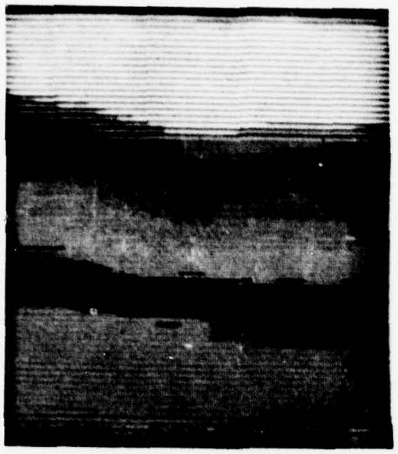

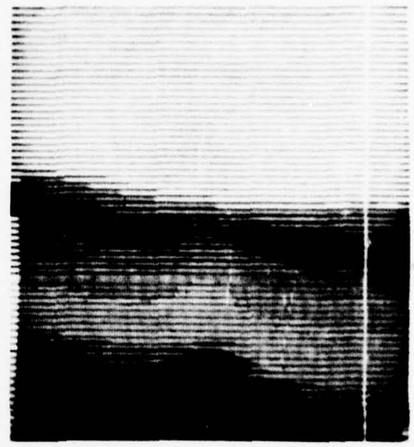

(0) GRAPHITE EPOXY
HEAT CONDUCTED FROM TOP EDGE

RADIATION/CONVECTION

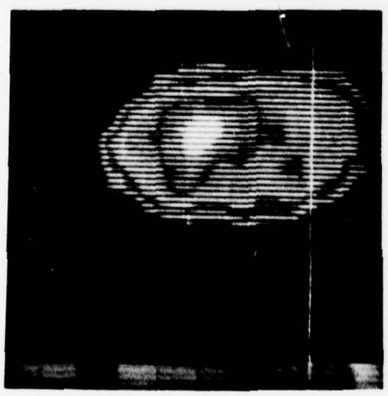

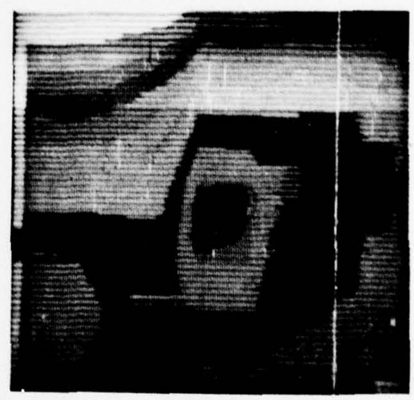

HEATED WITH HEAT GUN

COOLED WITH DAMP CLOTH

(0) GRAPHITE EPOXY

FIGURE 9 - PERTURBED ISOTHERM PATTERNS (TOP) AND "HOT SPOTS" (BOTTOM) AT PARTIAL THROUGH-HOLE ON BACK SURFACE, EATF

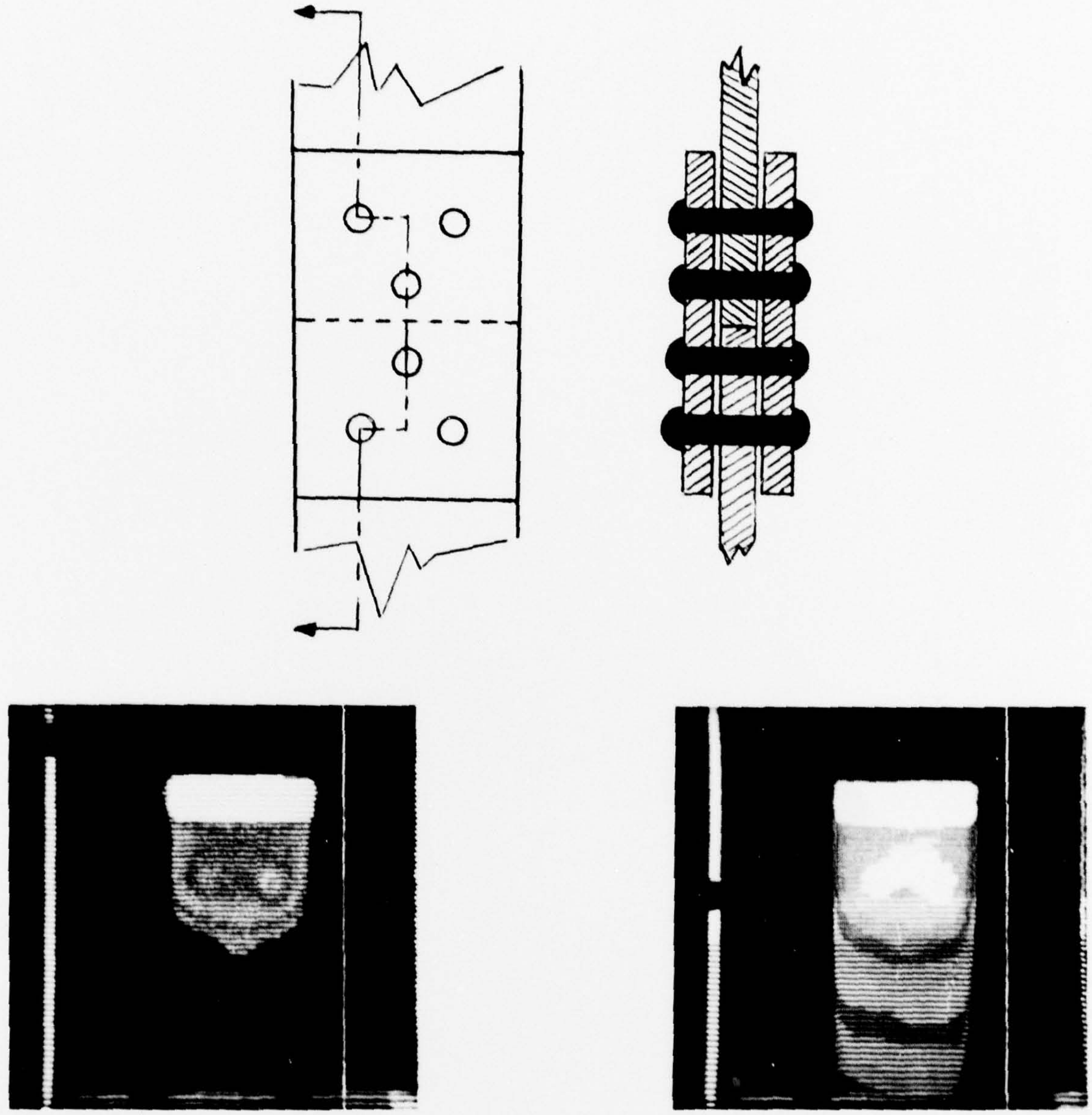

Note: White rectangle at top is the heated top half of main plate; grey area is cover plate on front. Note that only the top two rivets get hot, indicating a loose third rivet and air space between the main plate and cover plate.

FIGURE 10 - DRAWING AND INFRARED PHOTOGRAPHS OF IMPERFECTLY RIVETED ALUMINUM JOINT

(0/90) GLASS EPOXY
1/4" PARTIAL THROUGH-HOLE

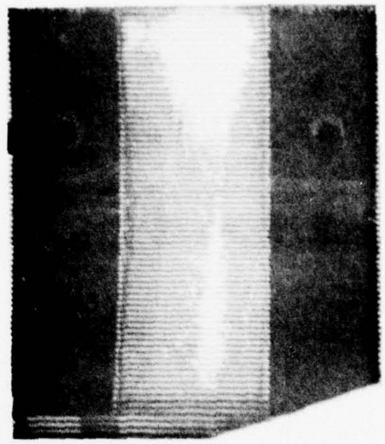

(0) GRAPHITE EPOXY AFTER AXIAL
CRACKING FROM 1/4" PARTIAL
THROUGH-SLIT

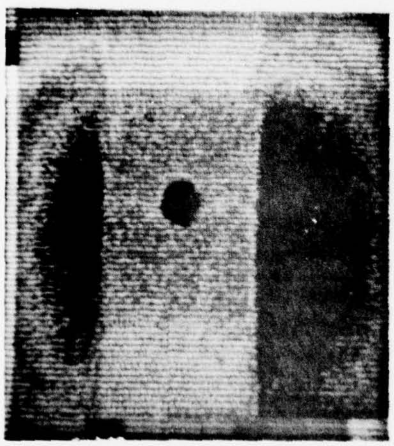

BEFORE AXIAL SPLIT

AFTER AXIAL SPLIT AT 0.3
STATIC ULTIMATE LOAD

(0) GRAPHITE EPOXY WITH 1/4" HOLE

FIGURE 11 - STRESS-GENERATED THERMAL FIELDS (SGTF) AT R = 0.1, 1 HZ

REFLECTIVITY

UNPAINTED ALUMINUM

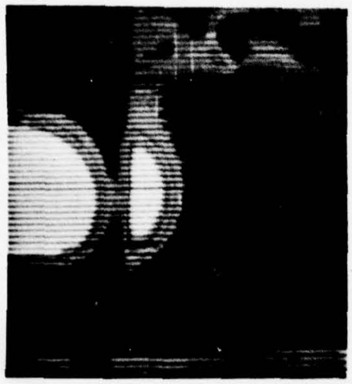

FINGER REFLECTION
WITH ISOTHERMS

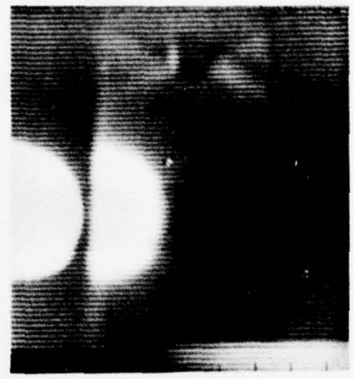

FINGER REFLECTION
WITH GRAY SCALE

CAR KEY REFLECTION
WITH ISOTHERMS

CAR KEY REFLECTION
WITH GRAY SCALE

FIGURE 12 - HEAT REFLECTED FROM UNPAINTED SURFACE OF 6061-T6 ALUMINUM SPECIMENS

EMISSIVITY

BLACK/WHITE PAINT ON ALUMINUM

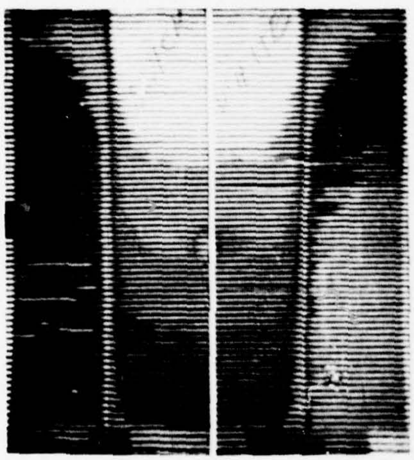

BLACK | WHITE

Heat conducted from the top. Note that black versus white paint shows no difference in emissivity.

REFLECTIVITY

BLACK/WHITE PAINT ON ALUMINUM

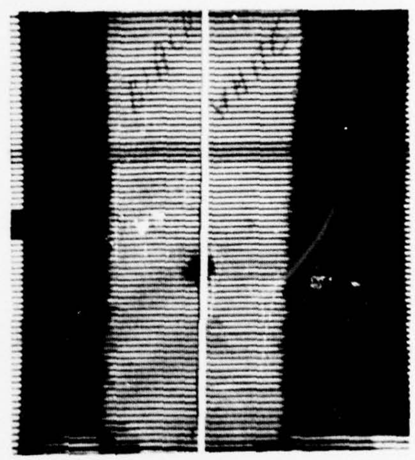

BLACK | WHITE

Attempted reflected body heat. Note that there is no reflection of body heat, unlike unpainted surfaces such as shown in Figure 12.

FIGURE 13 - EFFECT OF BLACK AND WHITE PAINT ON EMISSIVITY AND REFLECTIVITY OF ALUMINUM SURFACES

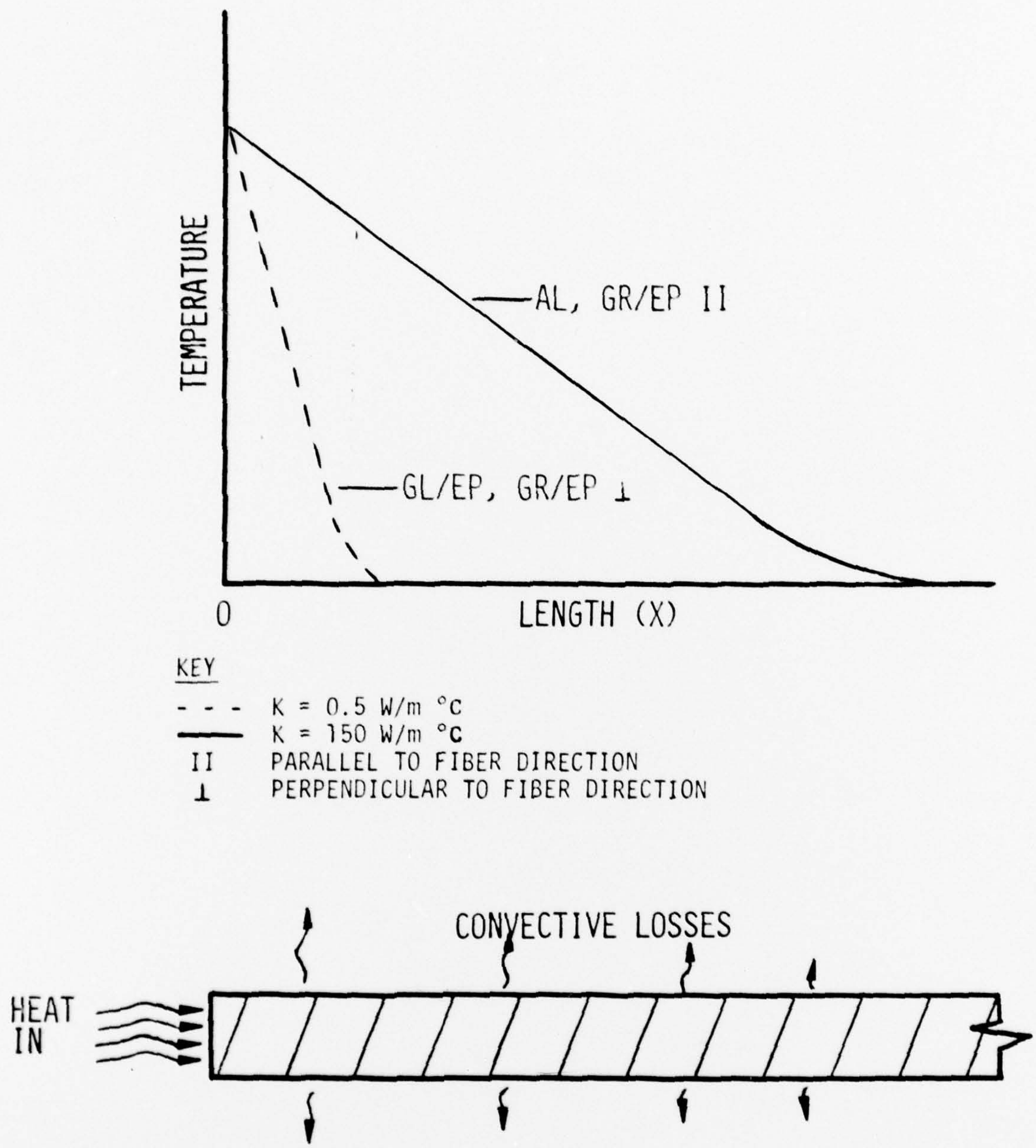

FIGURE 14 - TEMPERATURE VERSUS LENGTH ALONG WIDE PLATE HEATED AT X = 0

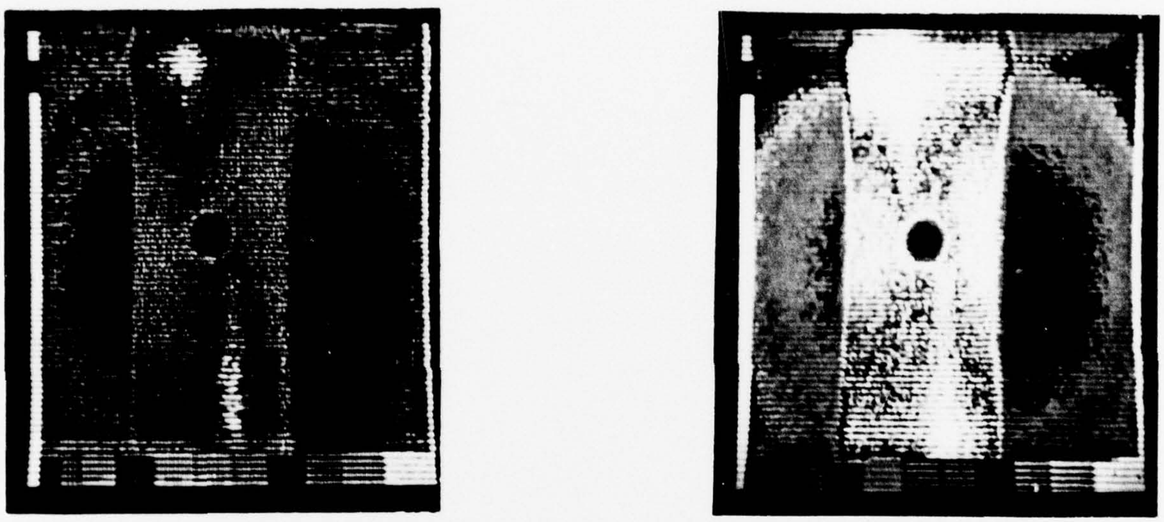

FIGURE 15 - BLACK AND WHITE VERSUS COLOR PHOTOGRAPHS OF COLOR VIDEOSCREEN RECORDED DURING SGTF TEST OF [0] GRAPHITE/EPOXY SHOWING "HOT SPOTS" ALONG CRACKED SURFACES EXTENDING FROM THE HOLE (THE PATTERN IS VISIBLE IN BOTH CASES)

SENSITIVITY

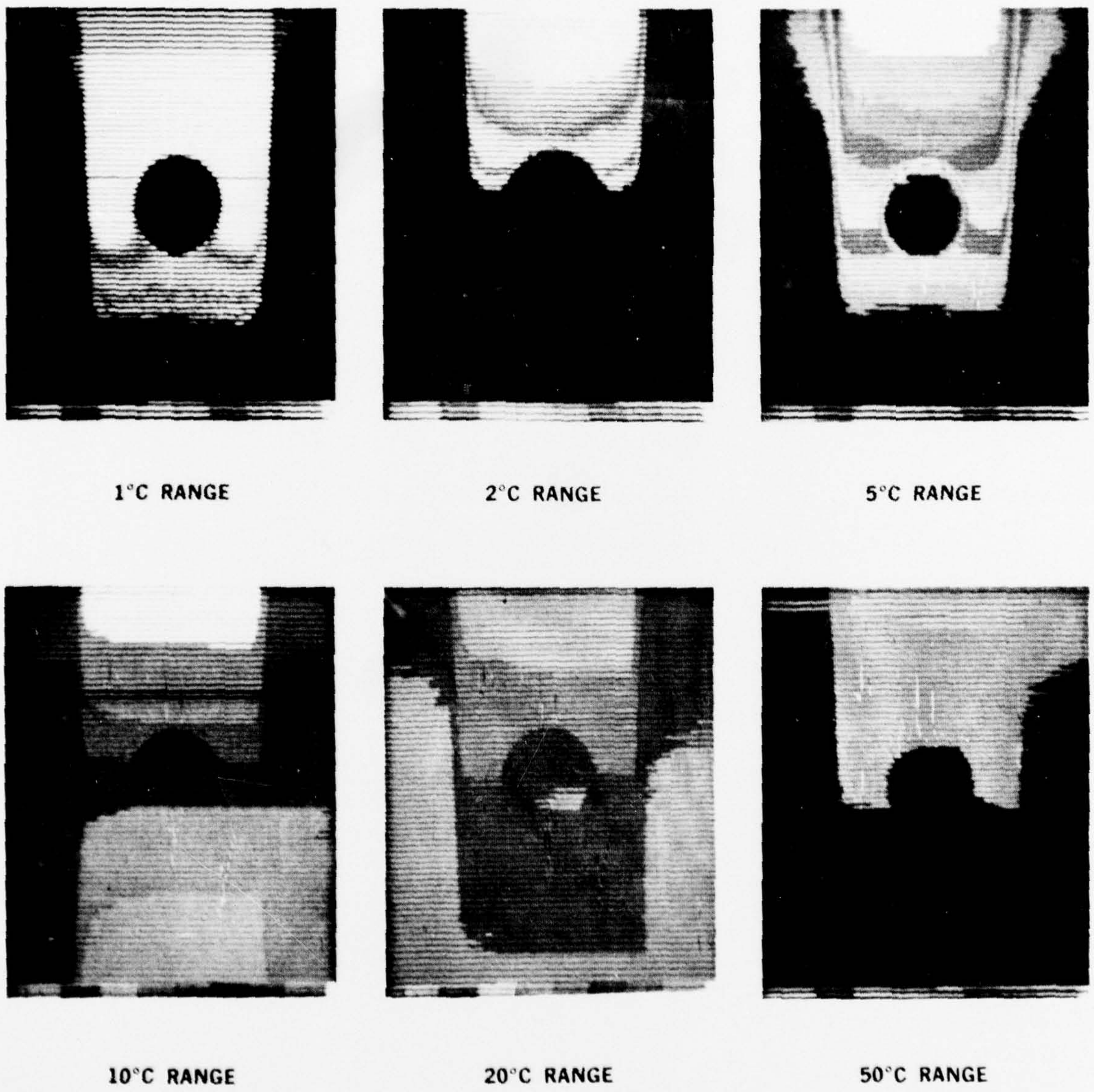

FIGURE 16 - COMPARISON OF VARYING IR CAMERA SENSITIVITY RANGES USED DURING EATF CONDUCTIVITY TESTS OF BLACK PAINTED ALUMINUM WITH 1/2-INCH-DIAMETER THROUGH-HOLE

HEAT SOURCE

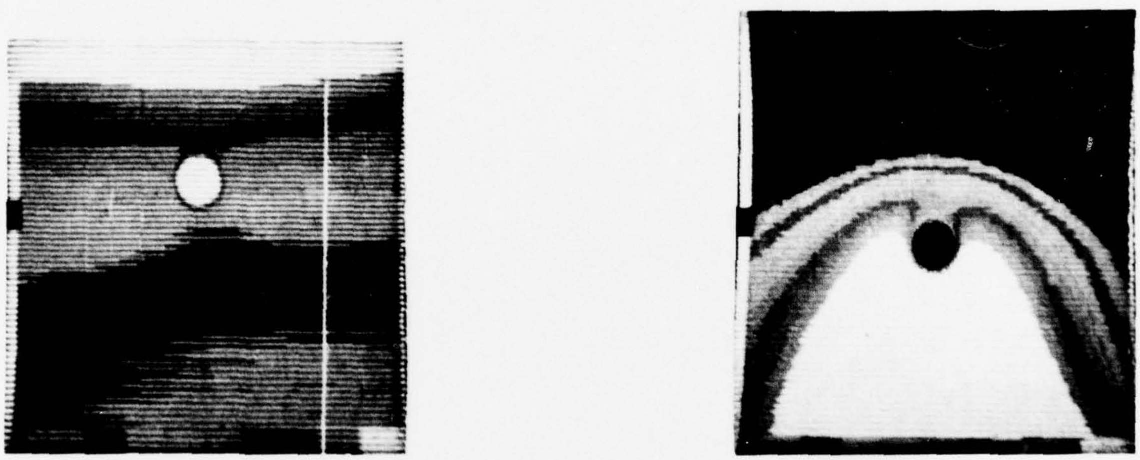

TOP OF PLATE HEATED BY STRIP HEATER

BOTTOM OF PLATE HEATED BY HEAT GUN

FIGURE 17 - COMPARISON OF HEAT APPLICATION TECHNIQUES SHOWING ISOTHERM PATTERNS AROUND [0] BORON/EPOXY WITH 1/4-INCH-DIAMETER (0.62 CM) THROUGH-HOLE

DISTRIBUTION LIST

NAVAIRENGCEN
1115
92A1B (2)
92713
92724 (20)
9011

NAVAIRDEVCEN 60633 (2)
NAVAIRPROCEN PE43
AFML/LLP
AMMRC DRXMR-MQ
NASA LANGLEY MS188E
NAVSHIP R&D Center (2803)

NAVAIR
AIR-340E (3)
AIR-5523 (2)
AIR-4114 (2)
AIR-5203 (2)
AIR-950D (2)

DDC -(12)

REVISION LIST

REVISION	PAGES AFFECTED	DATE OF REVISION